[2] Rizzi, A. W. and Inouye, M., "A Time-Split Finite-Volume Technique for Three-Dimensional Blunt-Body Flow," *AIAA Journal*, Vol. 11, No. 11, Nov. 1973, pp. 1478–1485.

[3] Kutler, P., Reinhardt, W. A., and Warming, R. F., "Multishocked, Three-Dimensional Supersonic Flowfields with Real Gas Effects," *AIAA Journal*, Vol. 11, No. 5, May 1973, pp. 657–664.

[4] Blottner, F. G. and Flugge-Lotz, I., "Finite Difference Computation of the Boundary-Layer with Displacement Thickness Interaction," *Journal de Mechanique*, Vol. 11, No. 4, 1964.

[5] Blottner, F. G., "Finite Difference Methods of Solution of the Boundary-Layer Equations," *AIAA Journal*, Vol. 8, No. 2, Feb. 1970, pp. 193–206.

[6] Lewis, C. H., "First Order Treatment of Higher-Order Boundary-Layer Effects," *The Physics of Fluids*, Vol. 13, No. 12, Dec. 1970, pp. 2939–2949.

[7] Davis, R. T., "Numerical Solution of the Hypersonic Viscous Shock-Layer Equations," *AIAA Journal*, Vol. 8, No. 5, May 1970, pp. 843–851.

[8] Davis, R. T., "Hypersonic Flow of a Chemically Reacting Binary Mixture Past a Blunt Body," AIAA Paper 70-805, Los Angeles, Calif., 1970.

[9] Jain, A. C. and Adimurthy, V., "Hypersonic Merged Stagnation Shock Layers, Part I: Adiabatic Wall Case," *AIAA Journal*, Vol. 12, No. 3, March 1974, pp. 342–347.

[10] Jain, A. C. and Adimurthy, V., "Hypersonic Merged Stagnation Shock Layers, Part II: Cold Wall Case," *AIAA Journal*, Vol. 12, No. 3, March 1974, pp. 348–354.

[11] Anderson, E. C. and Lewis, C. H., "Laminar or Turbulent Boundary-Layer Flows of Perfect Gases or Reacting Gas Mixtures in Chemical Equilibrium," CR-1893, 1971, NASA.

[12] Lewis, C. H., Anderson, E. C., and Miner, E. W., "Nonreacting and Chemically Reacting Turbulent Boundary-Layer Flows," AIAA Paper 71-597, Palo Alto, Calif., 1971; also *International Journal for Numerical Methods in Engineering*, Vol. 17, 1973, pp. 3–15.

[13] Lewis, C. H., Adams, J. C., and Gilley, G. E., "Effects of Mass Transfer and Chemical Nonequilibrium on Slender Blunted Cone Pressure and Heat Transfer Distributions at $M_\infty = 13.2$," TR-68-214, Dec. 1968, Arnold Engineering Development Center, Tullahoma, Tenn.

[14] Lewis, C. H. and Miner, E. W., "Stagnation Point Viscous Layers with Mass Transfer," *Computers and Fluids*, Vol. 2, No. 2, Aug. 1974, pp. 117–143.

[15] Pappas, C. C. and Lee, G., "Heat Transfer and Pressure on a Hypersonic Blunt Cone with Mass Addition," *AIAA Journal*, Vol. 8, No. 5, May 1970, pp. 954–956.

[16] Kang, S.-W. and Dunn, M. G., "Hypersonic Viscous Shock Layer with Chemical Nonequilibrium for Spherically Blunted Cones," *AIAA Journal*, Vol. 10, No. 10, Oct. 1972, pp. 1361–1362.

[17] Kang, S.-W., Jones, W. L., and Dunn, M. G., "Theoretical and Measured Electron-Density Distributions at High Altitudes," *AIAA Journal*, Vol. 11, No. 2, Feb. 1973, pp. 141–149.

[18] Kang, S.-W. and Dunn, M. G., "Hypersonic Viscous Shock Layer with Chemical Nonequilibrium for Spherically Blunted Cones," TR-AF-3093-A-1, Feb. 1972, Cornell Aeronautical Lab., Ithaca, N.Y.

[19] Dunn, M. G. and Kang, S.-W., "Theoretical and Experimental Studies of Reentry Plasmas," CR-2232, April 1973, NASA.

[20] Evans, J. S., Schexnayder, C. J., Jr., and Huber, P. W., "Boundary-Layer Electron Profiles for Entry of a Blunt Slender Body at High Altitudes," TN D-7332, July 1973, NASA.

[21] Browne, W. G., "Thermodynamic Properties of Some Atoms and Atomic Ions," MSD Engineering Physics TM2, General Electric Co., Philadelphia, Pa.

[22] Browne, W. G., "Thermodynamic Properties of Some Diatomic and Linear Polyatomic Molecules," MSD Engineering Physics TM3, General Electric Co., Philadelphia, Pa.

[23] Browne, W. G., "Thermodynamic Properties of Some Diatoms and Diatomic Ions at High Temperature," MSD Advanced Aerospace Physics TM8, May 1962, General Electric Co., Philadelphia, Pa.

[24] Blottner, F. G., "Non-Equilibrium Laminar Boundary Layer Flow of Ionized Air," Rept. R64SD56, Nov. 1964, General Electric Co., Philadelphia, Pa.

[25] Huber, P. W., Evans, J. S., and Schexnayder, C. J., Jr., "Comparison of Theoretical and Flight-Measured Ionization in a Blunt Body Re-Entry Flowfield," *AIAA Journal*, Vol. 9, No. 6, June 1971, pp. 1154–1162.

JANUARY 1975 AIAA JOURNAL VOL. 13, NO. 1

Buoyant Convection in Radiating Horizontal Fluid Layers

S. C. TRAUGOTT* AND S. H. YAMAMURA†
Martin Marietta Laboratories, Baltimore, Md.

Buoyancy-driven, two-dimensional convection in a horizontal layer of radiating fluid, confined between isothermal no-slip surfaces, is calculated with a numerical finite difference method. The radiation model was taken to be the grey Milne-Eddington approximation, and the formulation includes quite general radiative boundary conditions. Radiation is found to inhibit convection primarily due to increased stability. For the same ratio of Grashof to critical Grashof numbers, the flowfields are very similar with and without radiation. Convective heat flux can decrease the radiative flux below its static values. The radiative model employed resulted in essentially the same computing time both with and without radiation.

I. Introduction

BUOYANCY-driven convection occurs in horizontal fluid layers in a wide variety of situations. In many of these the characteristic length transverse to the layer, in the direction of gravity, is very much less than the distance along the layer. In such a geometry the thermal drive is related to the density variation across the layer, in contrast to situations in which the forcing is due to imposed horizontal gradients of density or temperature. There is then a stability problem, in addition to the question of the nature of the flow, once buoyant forcing is sufficient to overcome the inhibiting action of friction and heat conduction.

In many instances it is clear that radiative heat transfer also plays a role in the process. Such is the case with stellar convection, convection in a planetary atmosphere, and in laboratory experiments with certain fluids (carbon tetrachloride, ammonia). The role of radiative transfer in modifying critical conditions for the onset of convection has been the subject of considerable

Presented as Paper 74-9 at the AIAA 12th Aerospace Sciences Meeting, Washington, D.C., January 30–February 1, 1974; submitted February 15, 1974, revision received July 22, 1974. Work partially supported by the U.S. Air Force Office of Scientific Research (AFSC), under Contract F44620-71-C-0011.

Index categories: Radiatively Coupled Flows and Heat Transfer; Radiation and Radiative Heat Transfer.

* Principal Research Scientist, Mechanics Department. Associate Fellow AIAA.

† Senior Research Assistant, Mechanics Department.

theoretical attention.[1-6] Reference 2 includes experimental results. A recent survey by Spiegel[7] reviews some of this work as well as other investigations not mentioned here. Radiation acts in three distinguishable ways to modify stability. It provides an additional heat transfer mechanism, and this is a stabilizing influence. It modifies the initial hydrostatic temperature, usually by increasing the temperature gradient near solid boundaries, in which case this also stabilizes. Finally, it allows more general boundary conditions, and their influence can be in either direction. Clearly, radiation acts in a complex way to modify those conditions which just allow convection.

Almost nothing can be stated with certainty about the role of radiation once convection is established. The only relevant analysis known to us is in Ref. 3, which includes an approximate estimate of the modification of convective heat transport due to radiation. This approximation is optically thin and assumes the flow pattern to be that of linear stability theory. The result is a reduced convective flux for a fixed value of the excess in Grashof number above its critical value.

In this paper we describe an exploratory theoretical investigation of the role of radiative transfer in fully established two-dimensional buoyant convection, in a fluid layer contained between two infinite parallel horizontal surfaces. The governing equations are the unsteady Boussinesq equations of motion with a radiative heating term contained in the energy equation. This term is obtained from a grey differential (Milne-Eddington) model of radiative transfer. A grey assumption need not be fatal since there exist methods for relating a grey opacity to the opacity of a real, nongrey fluid. In particular, such a relation based on equating grey to nongrey radiative relaxation times appears promising.[8] The differential approximation is appropriate since the geometry involves no "shadow" effects which are now known to cause difficulties with differential methods. Use of this highly simplified radiation model was dictated by the lack of any other known method which would allow us to deal with finite resources with both the multi-dimensional aspect of radiative transfer and coupled fluid motions of the present case. We further note that the same differential model is also employed in the stability analyses of Refs. 4 and 6.

The system of equations is numerically integrated with respect to the two space coordinates and time. The method used is essentially Method V of Torrance.[9] The flow is assumed to be periodic in the horizontal direction with the period determined by maximizing the total vertical heat flux across the layer. Based on our calculations to date, we find no essential complications or increase in computing effort and expense above that of non-radiating calculations when our simplified model of radiation is included. This is one of the more important results of our study, since it implies that a rational radiation model could be incorporated into the numerical computation of much more complex flows, especially those relevant to atmospheric circulation, without undue increase in computing time. Incorporation of radiation into atmospheric flow models without the usual empirical and ad hoc basis is then limited only by the degree to which results such as those to be described turn out to be realistic.

II. Governing Equations

The geometry consists of two infinite horizontal planes separated by the vertical distance H. The lower surface is at temperature T_l, the upper at T_u. The Boussinesq approximation of the two-dimensional equations of motion, in a coordinate system with x the horizontal distance along the lower surface and y measured upwards from it, gives[10]

$$\partial U/\partial x+\partial V/\partial y = 0 \tag{1}$$

$$\frac{DU}{Dt} = -\frac{1}{\rho_o}\frac{\partial \Delta p}{\partial x} + \nu\nabla^2 U \tag{2}$$

$$\frac{DV}{Dt} = -\frac{1}{\rho_o}\frac{\partial \Delta p}{\partial y} + g\frac{\Delta T}{T_o} + \nu\nabla^2 V \tag{3}$$

$$\frac{D\Delta T}{Dt} + V\left(\frac{dT_s}{dy}+\Gamma\right) = \frac{k}{\rho_o C_p}\nabla^2\Delta T + \frac{\Delta Q}{\rho_o C_p} \tag{4}$$

Here ΔT and Δp are the departures of temperature and pressure from the hydrostatic case, for which temperature and pressure is $T_s(y)$ and $p_s(y)$. The same kind of definition holds for ΔQ, the local volumetric rate of heating attributable to the temperature field due to motion. Thus the temperature, pressure, and heating are given by $T = T_s(y)+\Delta T(x, y)$, $p = p_s(y)+\Delta p(x, y)$, and $Q = Q_s(y)+\Delta Q(x, y)$. The reference quantities ρ_o and T_o represent constant spatial averages of the corresponding variables, and Γ is the dry adiabatic lapse rate given by g/C_p, g being the gravitational acceleration. Without motion, the energy equation is

$$\frac{\partial T_s}{\partial t} = \frac{k}{\rho_o C_p}\frac{\partial^2 T_s}{\partial y^2} + \frac{Q_s}{\rho_o C_p} \tag{5}$$

Without volumetric heating the hydrostatic steady-state has a linearly decreasing temperature with height, but this no longer holds for the present study. Determination of the appropriate static temperature distribution is in fact no longer trivial, and in our calculations Eq. (5) was solved for it numerically. Once a steady solution of Eq. (5) is known, ΔT can be determined from an equation obtained by adding Eqs. (4) and (5), whose sum is

$$\frac{D\Delta T}{Dt} + V\left(\frac{dT_s}{dy}+\Gamma\right) = \frac{k}{\rho_o C_p}\left(\nabla^2\Delta T + \frac{d^2 T_s}{dy^2}\right) + \frac{Q}{\rho_o C_p} \tag{6}$$

The motivation for writing conservation of energy in form Eq. (6) is the nonlinear dependence of the total volumetric heating on temperature when this heating is radiative. It cannot then be conveniently decomposed into static and dynamic contributions. When Q, d^2T_s/dy^2, and Γ vanish, then Eq. (6) reduces to a more conventional form often used in numerical convection studies (see, for instance, Cabelli and Davis[11]).

In accounting for radiation we utilize an effective, spectrally averaged grey absorption coefficient, which is assumed constant at the value K. How this might vary with H and position to account for nongrey effects is not considered in this paper. With I_o the directionally averaged radiation intensity and $\mathbf{I}_1$ the radiative heat flux (negative if upwards), a radiative Q in Eq. (6) is given by (see, for instance, Traugott[14])

$$Q = \nabla\cdot\mathbf{I}_1 = K(I_o-4\pi B), \qquad \pi B = \sigma T^4 \tag{7}$$

A further relation between flux and averaged intensity is given by the Milne-Eddington approximation. This assumes the flux to be given by $\mathbf{I}_1 = (1/3K)\nabla I_o$.

We chose to work with I_o rather than the flux because it is a scalar quantity. It obeys the equation

$$\nabla^2 I_o = 3K^2(I_o-4\pi B) \tag{8}$$

This equation can be found in Refs. 6 and 14, or derived from Ref. 4. Equations (1–3, 6, 7, and 8) form a closed set which determines the velocity, temperature, and radiation fields. The set used in our computations results from the following manipulations.

Dimensionless variables are introduced with

$$\xi = x/H, \quad \eta = y/H, \quad \theta = (T-T_u)/(T_l-T_u)$$

$$u = UH/\nu, \quad v = VH/\nu, \quad \tau = t\nu/H^2, \quad i = I_o/4\sigma(T_l^4+T_u^4)$$

Use of a stream function ψ disposes of Eq. (1), while Eqs. (2) and (3) are combined into an equation for the vorticity Ω. The result, with Gr which is the Grashof number and equals $g(T_l-T_u)H^3/T_o\nu^2$, is

$$\frac{\partial\Omega}{\partial\tau} + \frac{\partial}{\partial\xi}(u\Omega) + \frac{\partial}{\partial\eta}(v\Omega) = Gr\frac{\partial\Delta\theta}{\partial\xi} + \nabla^2\Omega \tag{9}$$

where

$$u = \frac{\partial\psi}{\partial\eta}, \qquad v = -\frac{\partial\psi}{\partial\xi} \tag{10}$$

$$\Omega = \frac{\partial v}{\partial\xi} - \frac{\partial u}{\partial\eta} = -\nabla^2\psi \tag{11}$$

Equation (6) can be written in the form

$$\frac{\partial \Delta\theta}{\partial \tau}+\frac{\partial}{\partial \xi}[u(\Delta\theta+\theta_s+\gamma\eta)]+\frac{\partial}{\partial \eta}[v(\Delta\theta+\theta_s+\gamma\eta)]=$$
$$Pr^{-1}\left\{\nabla^2(\Delta\theta+\theta_s)+\frac{\lambda^2(1+n^4)}{4(1-n)}\left[i-\frac{[n+(1-n)\theta]^4}{(1+n^4)}\right]\right\} \quad (12)$$

where

$$\gamma=\frac{gH}{C_p(T_l-T_u)},\quad \lambda^2=3K^2H^2\chi,\quad \chi=\frac{16\sigma T_l^3}{3Kk},\quad n=\frac{T_u}{T_l}$$

The somewhat elaborate appearance of Eq. (12) comes from the conservative form of the convection terms which is advantageous for numerical purposes (see, for instance, Emmons[12]). These terms contain γ although it is possible and perhaps more conventional to eliminate its occurrence there by working with potential temperature. This would then cause the adiabatic lapse rate to appear in the definition of the Grashof number. However, in the present case γ would appear also in the radiation term. For this reason potential temperature is not used here. Quantities i and θ are further related by the dimensionless version of Eq. (8), or

$$\nabla^2 i=3K^2H^2\left[i-\frac{[n+(1-n)\theta]^4}{(1+n^4)}\right] \quad (13)$$

Equation (12) is to be regarded as an equation for $\theta=\Delta\theta+\theta_s$ where θ_s is known. The latter comes from a separate calculation of θ_s and i_s obtained by following to a steady-state simultaneous solution of Eq. (13) and the dimensionless version of Eq. (5), or

$$\frac{\partial \theta_s}{\partial \tau}=Pr^{-1}\left\{\frac{\partial^2\theta_s}{\partial\eta^2}+\frac{\lambda^2(1+n^4)}{4(1-n)}\left[i_s-\frac{[n+(1-n)\theta_s]^4}{(1+n^4)}\right]\right\} \quad (14)$$

This calculation determines the initial radiative-conductive state in which, if it is sufficiently unstable to gravitational overturning, convection then develops. For this static state the heat flux across the layer in the η (or y) direction is made up of contributions from conduction and radiation, and in the original dimensional variables this is $q_{ys}=-k(dT_s/dy)-(1/3K)(dI_{os}/dy)$.

We make the heat flux dimensionless in the usual way with the purely conductive flux, and then the hydrostatic Nusselt number is given by

$$Nu_s=\frac{Hq_{ys}}{k(T_l-T_u)}=-\left[\frac{d\theta_s}{d\eta}+\frac{\lambda^2}{12K^2H^2}\frac{(1+n^4)}{(1-n)}\frac{di_s}{d\eta}\right] \quad (15a)$$

This is unity only without radiation, or the second term on the right. In general, with convection, the transverse heat flux is given by

$$q_y=-k\frac{\partial T}{\partial y}-\frac{1}{3K}\frac{\partial I_o}{\partial y}+\rho_o C_p V(T-T_o)$$

This depends on both space coordinates. The horizontally averaged transverse heat flux is of interest, and with our periodicity assumption this is obtained by averaging over the horizontal width of a single convection cell, denoted by L. The nondimensional result is

$$Nu=-\frac{1}{l}\int_0^l\left[\frac{\partial\theta}{\partial\eta}+\frac{\lambda^2}{12K^2H^2}\frac{(1+n^4)}{(1-n)}\frac{\partial i}{\partial\eta}-Pr\,v\theta\right]d\xi \quad (15b)$$

where $l=L/H$.

Equation (15b) serves to define the conductive, radiative, and convective contributions to the total heat flux by writing it as $Nu=Nu_\theta+Nu_i+Nu_v$.

Boundary Conditions

Equations (9–14) were used to determine the flow, temperature, and radiation fields. Assuming horizontal periodicity over a length $2l$, symmetry boundary conditions at $\xi=0$ and $\xi=l$ (the width of a single convection roll) are $\psi=\partial^2\psi/\partial\xi^2=\partial\Delta\theta/\partial\xi=\partial i/\partial\xi=0$. Only small departures from symmetry are reported by Cabelli and Davis[11] from calculations with more general periodic boundary conditions. As already mentioned, l is an unknown which was determined to be that which maximizes Eq. (15b). The justification for this even without radiation is mostly metaphysical (see a brief description in Ref. 13). With radiation included, the only justification is that no other procedure comes readily to mind, and that the results obtained seem reasonable and in agreement with what is known about the influence of radiation from linear stability analysis. All our results to date were obtained with no-slip conditions on the horizontal boundaries, hence at $\eta=0,1$: $\psi=\partial\psi/\partial\eta=\Delta\theta=0$; $\theta_s(0)=1$, $\theta_s(1)=0$.

Radiative boundary conditions must be consistent with the Milne-Eddington approximation. For black walls the appropriate conditions are given by Eq. (13) of Ref. 14. A generalized version is given below, obtained as follows. In Ref. 15 boundary conditions are derived which are consistent with a two-stream (or Schuster-Schwarzschild) method. This method is essentially the same as the Milne-Eddington approximation, with only a minor difference in a particular numerical factor. Equation (9) of Ref. 15 contains the emissivity of a nontransmitting surface. In the present notation, this boundary condition is, for the upper surface with emissivity ε_u:

$$\frac{\partial i}{\partial\eta}=-\frac{2KH\varepsilon_u}{2-\varepsilon_u}\left[i(\xi,1)-\frac{n^4}{1+n^4}\right] \quad (16a)$$

(for Schuster-Schwarzschild). Equation (13) of Ref. 14, for $\varepsilon=1$, can be correspondingly written as

$$\frac{\partial i}{\partial\eta}=-(3)^{1/2}KH\left[i-\frac{n^4}{1+n^4}\right] \quad (16b)$$

(for Milne-Eddington).

It is not difficult to generalize the analysis of Ref. 15 to allow transmitting surfaces and to derive boundary conditions for the Schuster-Schwarzschild method which include a transmissivity t. Space does not permit inclusion of this derivation. One finds that any radiation incident on the surface from the outside enters the formulation, and this radiation was assumed to be isotropic with intensity $\sigma T_R{}^4/\pi$, T_R being an effective reservoir black body temperature for any such external radiation source. The result is a generalization of Eq. (16a). Based on a comparison between Eq. (16a) and (16b) for a black surface, we replace the corresponding factor 2 in our generalized derivation with $(3)^{1/2}$, finally arriving at compatible boundary conditions to be used with Eq. (13):

$$\eta=0:\quad \frac{\partial i}{\partial\eta}=\frac{(3)^{1/2}KH}{2-\varepsilon_l-t_l}\left[(\varepsilon_l+t_l)i-\frac{(\varepsilon_l+t_l s^4)}{1+n^4}\right]$$
$$\eta=1:\quad \frac{\partial i}{\partial\eta}=-\frac{(3)^{1/2}KH}{2-\varepsilon_u-t_u}\left[(\varepsilon_u+t_u)i-\frac{(\varepsilon_u n^4+t_u m^4)}{1+n^4}\right] \quad (17)$$

Below the lower boundary, upward radiation is radiated from a reservoir at temperature $T_{-\infty}=sT_l$. Above the upper boundary, corresponding downward radiation comes from another reservoir at $T_\infty=mT_l$. Obviously, these effects disappear for nontransmittiong opaque surfaces with $t=0$. Their inclusion allows much greater versatility in generating a quite general initial static temperature distribution structured by conduction and radiation.

III. Analytical Considerations

Even to compute only the radiative-conductive state, from Eqs. (13, 14 and 17), is not a trivial matter. Some insight can be obtained for the case of λ, but not KH, large. Then radiation dominates conduction but is not optically thick. Here the temperature profile is given essentially by radiative equilibrium, with vanishing right-hand sides of Eqs. (13) and (14) and i linear in η. Conduction will only act to prevent radiative slip at the boundaries by structuring large temperature gradients there. The average intensity and temperature are conveniently written as

$$(1+n^4)i=D_1\eta+D_2,\quad \theta=[(D_1\eta+D_2)^{1/4}-n]/(1-n)$$

The temperature slip at lower and upper walls, respectively, is

$$\eta=0:\quad \theta_w(0)-\theta(0)=1-\theta(0)=(1-D_2{}^{1/4})/(1-n)$$
$$\eta=1:\quad \theta(1)-\theta_w(1)=\theta(1)=[(D_1+D_2)^{1/4}-n]/(1-n)$$

From Eqs. (17), D_1 and D_2 are determined to be

$$D_1 = (3)^{1/2}KH[(D_3 - D_4)/D_5]$$

$$D_2 = \left(\frac{2}{\varepsilon_l + t_l} - 1\right)\frac{D_3}{D_5} + \left(\frac{2}{\varepsilon_u + t_u} - 1 + (3)^{1/2}KH\right)\frac{D_4}{D_5}$$

with

$$D_3 = (\varepsilon_u n^4 + t_u m^4)/(\varepsilon_u + t_u), \quad D_4 = (\varepsilon_l + t_l s^4)/(\varepsilon_l + t_l)$$

$$D_5 = 2/(\varepsilon_l + t_l) + 2/(\varepsilon_u + t_u) - 2 + (3)^{1/2}KH$$

An illustration with atmospheric relevance is a hot black lower surface (the ground) and a completely transmitting cooler upper surface (the interior of a strong inversion of limited vertical extent). Suppose further that above the inversion the temperature is very low, so that one has essentially no thermal radiation entering the region of interest from above. For this example $\varepsilon_l = 1$, $t_l = 0$, $\varepsilon_u = 0$, $t_u = 1$, and $m = 0$. This gives

$$D_1 = -(3)^{1/2}KH/(2 + 3^{1/2}KH)$$

$$D_2 = 1 + (3)^{1/2}KH/(2 + 3^{1/2}KH)$$

$$\theta(1) - \theta_w(1) = [2 + (3)^{1/2}KH]^{-1/4} - n/(1 - n)$$

The lower surface slip is positive, as usual. But the upper surface slip can be substantially negative. For instance, with $(3)^{1/2}KH = 1$ and $n = (1 + 3^{-1/4})/n$, the upper temperature slip is -1. One concludes that temperature profiles quite different from those between opaque and solid surfaces are possible with our model from various choices of the available parameters. Allowing for conduction, one can predict that the temperature profile for this particular example will be strongly unstable to convection near the bottom and strongly stable near the top. The width and nature of the interior layer depends, of course, on λ. Detailed profiles can and have been obtained from numerical analysis, as will be described in Sec. V.

IV. Finite Difference Method

Equations (9–14) were written in finite difference form and then programed, incorporating the boundary conditions, and solved on an IBM 370/155 remotely accessed computer. The finite difference approximations were those of Method V of Ref. 9. The scheme is explicit and uses: forward time differences; three-point, noncentral forward or backward differences with direction depending on velocity for the (conservative) convection terms; three-point central differences for first space derivatives; three-point central differences for second space derivatives. Successive over-relaxation is used, with a relaxation parameter determined from a formulation given by Young.[16] As far as possible we followed the procedures described by Torrance.[9,17] We included certain of his shortcuts in which not all relaxation iterations are performed at every time step early in the flow development, and in which ψ and i updates to Ω and θ are not performed at every time step when the flow has nearly attained its asymptotic steady-state. The occurrence of i and its governing Eq. (13) is of course a new feature in our model and merits a brief discussion.

In the sequence of operations the average intensity i was treated in relation to θ in an analogous fashion to ψ as related to Ω. Thus, suppose an advance in time has given a new temperature field from Eq. (12) and then a new vorticity field from Eq. (9). The updated ψ field from Eq. (11) for the new Ω, obtained by the relaxation method, is then followed by a corresponding relaxation of Eq. (13) for an updated radiation field for the new θ. Nothing essentially different is introduced into the calculation scheme by the radiation field since Eq. (13) is elliptic just as is Eq. (11). This, of course, is the principal advantage in the use of the Milne-Eddington approximation. In fact, we found no significant difference in running time between flows with and without radiation. Time step size restrictions are identical to those of the nonradiating problem, depending only on the velocity field and mesh size, since the radiation field does not explicitly depend on time.

The initial static state was obtained by relaxing Eq. (13) in conjunction with the full unsteady version of Eq. (14). This calculation was started with a pure conduction temperature profile and a radiative equilibrium profile for i.

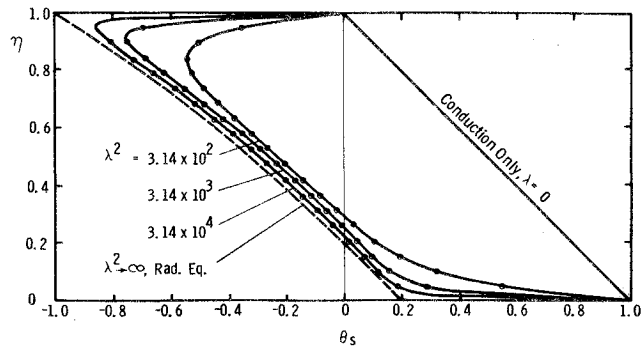

Fig. 1 Static temperatures, transmitting upper and black lower surface, $m = 0$, $n = 0.88$, $KH = 3^{-1/2}$.

The convective motion was started with a selected l and a small sinusoidal temperature perturbation located at $\eta = \frac{1}{2}$, turned on only initially. The solution then grew in time if the static state was convectively unstable, in our limited examples to date always to a steady state. The optimum cell width was determined by stretching or shrinking l and beginning a new calculation with an input from the previous solution. This technique was also used to obtain the flow at one Grashof number from that at another. Further, we used this technique in a stability study to determine Gr_c, the critical Grashof number. This was done by greatly reducing by a fixed factor (10^{-3}) the flowfield and $\Delta\theta$ already calculated at some supercritical Gr, and then following the subsequent temporal evolution of this scaled-down solution. This would soon either grow or decay exponentially except at a particular Grashof number, which we took to be Gr_c. This search for Gr_c required far less time than one initiated by only a small initial temperature disturbance and no flow.

All results reported in this paper were obtained with a 20×20 mesh grid applied to a single convective cell. Typically, solutions for four values of l, sufficient to locate the maximum heat flux, and a final run to obtain the maximized solution, were obtainable for about 600 (1973) dollars. All calculations are for $Pr = 1$ and $\gamma = 0$. A comparison of computing time between radiating and nonradiating convection can be made as follows. As steady state is approached and only one or two relaxation iterations are necessary, a typical nonradiative calculation required 124 sec to cover a time interval of $\Delta\tau = 0.16$. With radiation, the same time interval took 182 sec of computer time.

V. Numerical Results

Initial Static State

An example of a static calculation which illustrates the effect of a transmitting surface is shown in Fig. 1. The surface parameters are those of the example discussed analytically in Sec. III. The numerical calculation shows, as anticipated, progressively more narrow conduction boundary layers with increasing λ. This case serves to establish confidence in our numerical method of integrating Eq. (13), since the results appear to tend properly towards the analytically established radiative equilibrium limit ($\lambda \to \infty$). The profiles depart radically from the pure conduction limit, $\lambda = 0$, and show how temperature profiles of atmospheric interest can be produced by our very simple model. No convective calculations have as yet been made for this case.

All radiative-convective calculations to date were done with the much more conventional static temperature profile of Fig. 2. Here both upper and lower surfaces are black, and a not very large λ^2 of 31.4 was chosen to avoid very narrow conduction layers. The optical thickness of the layer is again $KH = 3^{-1/2}$, neither large nor small. The temperature profile is typically S shaped. The corresponding heat flux profiles are given in Fig. 3.

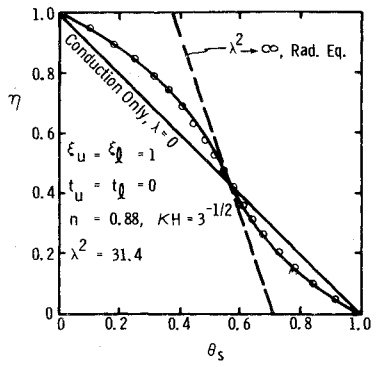

Fig. 2 Static temperatures, both surfaces black.

The radiative flux is larger than the conductive by a factor of roughly 9. Both temperature and radiative heat flux qualitatively resemble experimental profiles in carbon tetrachloride shown in Figs. 82 and 83 of Ref. 18.

Conditions for the Onset of Convection

Knowledge of critical values of Gr, or Gr_c, is very helpful in the interpretation of convective motion. In Fig. 4 we show a composite plot which summarizes what we have found for the effect of radiation both on neutral stability conditions and convection in supercritical conditions. The lower portion of Fig. 4 gives Gr_c as a function of l, the horizontal nondimensional cell width. The dashed curve comes from the classical result of linear stability analysis which gives Gr_c as a function of disturbance wave number, for no-slip surfaces. As is well known, the minimum is at $Gr_c = 1707$ and, in our notation, $l = 1.008$. The X on the curve is the result of our numerical search, at $l = 1$, for that Gr for which a small disturbance will neither grow nor decay. This gave a Gr_c of 1700 ± 15, another accuracy check on our numerical work. With radiation, Gr_c is considerably increased, and our determination of the minimum for $\lambda^2 = 31.4$, $KH = 3^{-1/2}$ is $Gr_c = 5100 \pm 100$ at $l_c = 0.850 \pm 0.025$. The slightly lower certainty here results from the need to search for l_c. This increase in Gr_c and decrease in l_c agrees qualitatively with results in Refs. 3 and 6. A quantitative comparison was not possible due to differences in choice of parameters; at best one can say that for our conditions a crossplot of results given in Ref. 6 gives $4000 < Gr_c < 6800$.

Developed Convection

Asymptotically steady, finite amplitude convection was calculated for four cases, where a case is defined to include a search for the optimizing cell width. One can interpret the four examples physically in terms of an experiment in which a variation in gravity is available (a centrifuge). A given container with different but fixed wall temperatures could contain two fluids, identical in all respects except that one but not the other is strongly absorbent to thermal radiation. One could increase Gr for the nonradiating fluid by speeding up the centrifuge. Then,

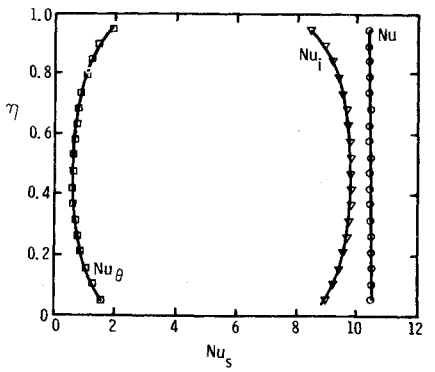

Fig. 3 Static heat fluxes, both surfaces black, $n = 0.88$, $\lambda^2 = 31.4$, $KH = 3^{-1/2}$.

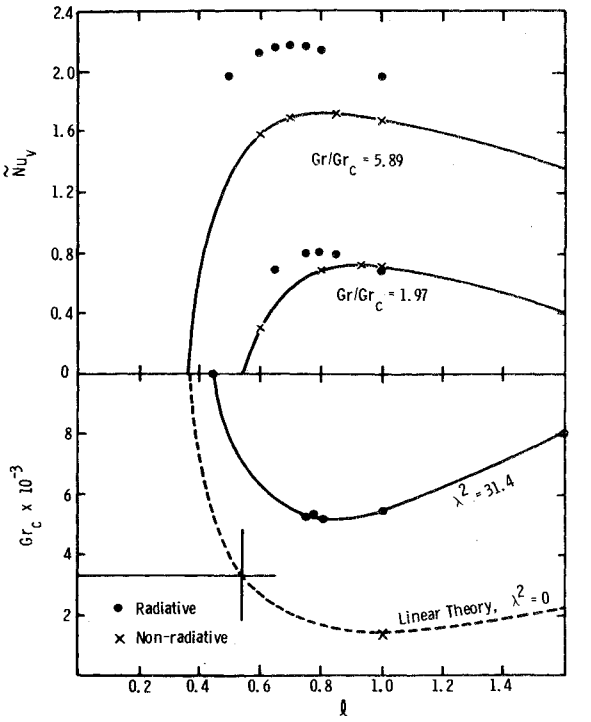

Fig. 4 Neutral stability and supercritical convective heat flux.

at fixed speed, one could substitute the radiating fluid to produce the necessary λ^2 at fixed Gr. Finally, the speed could again be increased with the radiating fluid. The four cases have Grashof numbers of 3.35×10^3 and 1×10^4 without radiation, and $Gr = 1 \times 10^4$, 3×10^4 with radiation. Both radiating examples have the values of λ^2 and KH used just above. The rationale for our choice of Gr was that, for the values of Gr_c given just above, one then has only two values of Gr/Gr_c, both with and without radiation. These are 1.97 and 5.89. As will be seen, it is this ratio upon which convection appeared primarily to depend. This conclusion follows from the upper part of Fig. 4.

We have shown there a measure of the vertically averaged convective flux as a function of l, both with and without radiation. This measure is $\tilde{N}u = \bar{N}u - \bar{N}u_s$, obtained by subtracting the vertically averaged dimensionless static flux from the total flux. Without radiation, of course, $\bar{N}u_s = 1$. Our radiative examples have $\bar{N}u_s = 10.41$. With radiation the quantity $\tilde{N}u$ is not identical to the vertically averaged convective flux but was found to be somewhat smaller. This is because $\bar{N}u_i \neq \bar{N}u_{is}$. Based on the limited data available it appeared that the most effective way of incorporating radiation into the variation of intensity of convection with thermal driving, was to use $\tilde{N}u$ and Gr/Gr_c. The solid curves were drawn to pass through the x symbols which represent radiationless calculations, and vanish at values of l given by critical conditions as shown in the lower portion of the figure. The circled x symbols represent our radiative calculations. Note that the circled symbol on the l axis is relevant to both

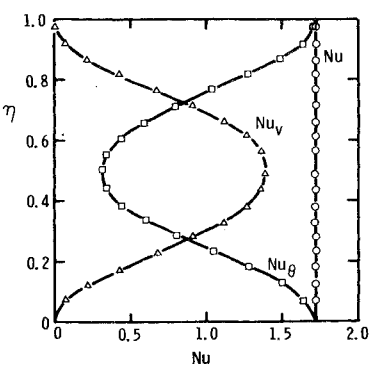

Fig. 5 Nonradiative heat fluxes, $Gr = 3350$.

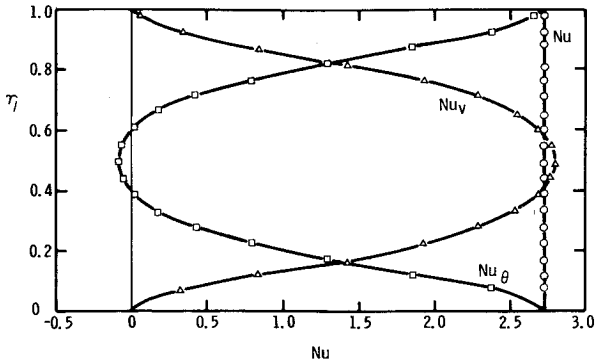

Fig. 6 Nonradiative heat fluxes, $Gr = 10{,}000$.

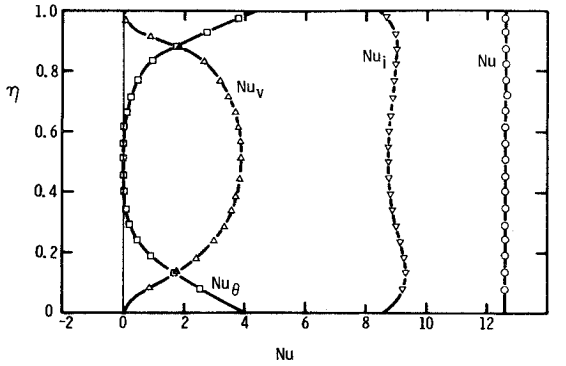

Fig. 8 Heat fluxes in a radiating layer, $Gr = 30{,}000$, $n = 0.88$, $KH = 3^{-1/2}$, $\lambda^2 = 31.4$.

lower and upper portions of the figure if one identifies absence of convection with critical stability conditions.

Several things are of interest. Radiation decreases the maximizing l. This conclusion is obvious when the comparison is made at the same value of Gr/Gr_c, but even at the same Gr (1×10^4), the lower set of radiative data seem to peak at a slightly lower cell width than the upper solid curve. This radiative lowering of optimum cell width for finite amplitude convection agrees with the linear stability trend of decreasing l_c with radiation discussed earlier. Further, while it is true that at a given value of Gr radiation drastically decreases convection, this is primarily an effect of an increase in stability. Most of this effect disappears when a comparison is made between radiating and nonradiating flows at the same value of Gr/Gr_c, and on this basis radiation results in a slight to moderate increase in convection, or at least our measure of it.

Figures 5–8‡ show details of the vertical flux distribution, for the four cases, evaluated at the optimum l. These were taken to be, respectively, $l = 0.93$, 0.85, 0.79, and 0.70 for $Gr = 3.35 \times 10^3$ and 1×10^4, $\lambda^2 = 0$; $Gr = 1 \times 10^4$ and 3×10^4, $\lambda^2 = 31.4$. Thus the four steps in the imaginary sequence of experiments described above lead to a monotonic decrease of cell width. The nonradiating examples, Figs. 5 and 6, show nothing not already known. Surface values have been extrapolated from data at interior points, subject to the constraint of constant total flux. The interior calculated flux is constant to about one part in 10^4. Radiative convection is shown in Figs. 7 and 8. These, taken together with the corresponding hydrostatic heat balance of Fig. 3, illustrate the development of progressively more intense convection, from rest to Grashof numbers of 1×10^4 and 3×10^4. One sees, as expected, the total heat flux across the layer increasing with increasing convection, and progressively less conduction in the interior of the layer, just as without radiation.

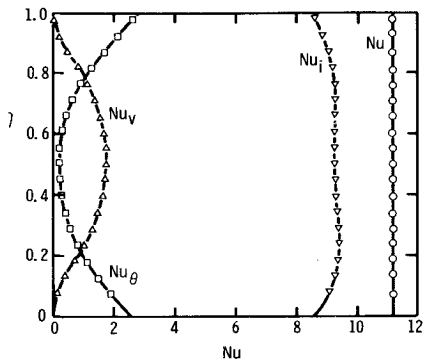

Fig. 7 Heat fluxes in a radiating layer, $Gr = 10{,}000$, $n = 0.88$, $KH = 3^{-1/2}$, $\lambda^2 = 31.4$.

‡ These figures in an earlier preprint version of this paper exhibit noticeable vertical variations of total heat flux. This was due to inconsistent evaluation of the last term in Eq. (15b), and this has been corrected. We acknowledge the prodding of a reviewer.

A slight amount of "counter-gradient" conduction was found in the center at the higher Grashof numbers both with and without radiation. An interesting effect is the reduction of radiative flux below its hydrostatic distribution due to convection. The effect is not very large, but then neither are our largest values of Gr. It would be interesting to see to what extent very intense motion could carry the entire burden of heat transport in the interior of convecting layers, at large Gr, even in presence of radiation.

Detailed features of our solutions are shown in Figs. 9–12, corresponding to the examples of Figs. 5–8. Only half of a cell pair is shown. The plots were obtained on a Calcomp 665 plotter. Each of these figures displays, from left to right, lines of constant ψ, Ω, θ, and, with radiation, i. All contours for these variables are normalized to divide the difference between maximum and minimum of the respective functions into 10 intervals. The contours of constant vorticity need interpretation. The circulation in these flows is upwards on the left and downwards on the right, as can be seen from the isotherms. This corresponds to vorticity opposite in sign to that induced by friction on the no-slip walls, hence the vertical vorticity distribution shows a sign reversal which manifests itself as a mainly horizontal dividing line in a vorticity contour plot. This can be used as a convenient qualitative measure of boundary-layer thickness. Our vorticity contour normalization was based on these wall, rather than interior, vorticities.

The nonradiating flow in Fig. 9 and the radiating flow in Fig. 11 correspond to the same (lower) value of Gr/Gr_c, and Fig. 4 shows that they have nearly the same convective flux. A comparison was made between them by re-plotting the contours of Fig. 9 to the same horizontal length scale as that in Fig. 11. The contours are then nearly indistinguishable, despite their large discrepancy in Gr. For the radiating examples contours of constant average intensity, i, are very nearly horizontal. Since i is a potential for the radiative flux, this means that the horizontal

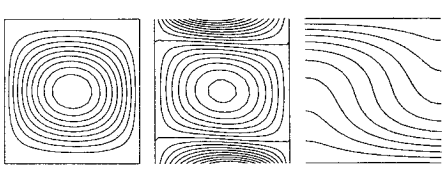

Fig. 9 Nonradiating solutions, $Gr = 3350$.

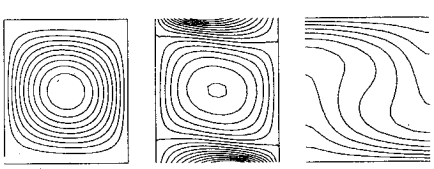

Fig. 10 Nonradiating solutions, $Gr = 10{,}000$.

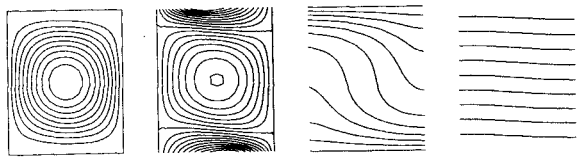

Fig. 11 Radiating solutions, $Gr = 10{,}000$.

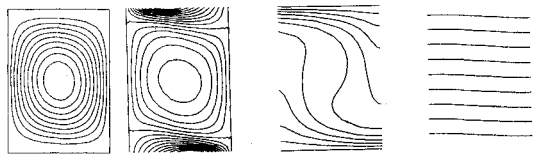

Fig. 12 Radiating solutions, $Gr = 30{,}000$.

flux in our examples is far less than the vertical flux despite the fully two-dimensional nature of the temperature field. Here it is important to remember the limited extent of our examples, in particular with respect to optical depth. If this quasi-one-dimensional feature were to hold generally, it might serve to justify one-dimensional radiative modeling in flows such as these and be a result of some importance.

VI. Summary and Conclusions

The following conclusions can be drawn from this study, although their general validity has clearly not been established by our very limited choice of examples and parameters. Radiation strongly inhibits buoyancy driven convection in a horizontal fluid layer. Most of this effect appears to be due to radiative modification of the neutral stability boundary. When flows with and without radiation are compared at the same ratio of Grashof to critical Grashof numbers, they then exhibit convective heat fluxes that are qualitatively the same, but at a reduced cell width. Convective heat flux appears to grow with increasing Grashof number, at the expense of both conduction and radiative flux in the interior of the layer. With a fully two-dimensional radiative model and temperature field, the calculated radiation field is nevertheless essentially one dimensional for an optical depth chosen to be neither very small nor very large.

These results were obtained for only one radiative-conductive initial state, with a temperature distribution not drastically different from the purely conductive linear profile. Our model, as shown, in Fig. 1, permits much more radical departures, and an investigation of convection in such cases, for a variety of optical depths, appears to be the obvious direction for further work.

References

[1] Goody, R. M., "The Influence of Radiative Transfer on Cellular Convection," *Journal of Fluid Mechanics,* Vol. 1, Pt. 4, Oct. 1956, pp. 424–435.

[2] Gille, J. and Goody, R. M., "Convection in a Radiating Gas," *Journal of Fluid Mechanics,* Vol. 20, Pt. 1, Sept. 1964, pp. 47–79.

[3] Christophorides, C. and Davis, S. H., "Thermal Instability with Radiative Transfer," *Physics of Fluids,* Vol. 13, No. 2, Feb. 1970, pp. 222–226.

[4] Niederdrenk, P., "Thermoconvective Instability in a Radiating and Conducting Fluid" (in German), *Zeitschrift fuer Angewandte Mathematik und Mechanik,* Vol. 52, No. 2, Feb. 1972, pp. 85–92.

[5] Wang, P. H. and Gille, J., "Radiative Stabilization of Bénard Convection with Black and Mirror Boundaries," *Conference on Atmospheric Radiation,* (American Meteorological Society, Boston), 1972, pp. 276–279.

[6] Arpaci, V. S. and Gözüm, D., "Thermal Stability of Radiating Fluids: The Bénard Problem," *Physics of Fluids,* Vol. 16, No. 5, May 1973, pp. 581–588.

[7] Spiegel, E. A., "Convection in Stars II. Special Effects," *Annual Review of Astronomy and Astrophysics,* Vol. 10, 1972, pp. 261–304 (Annual Reviews Inc., Palo Alto, Calif.).

[8] Dudis, J. J. and Traugott, S. C., "The Effect of Radiative Transfer on Shear-Flow Instability in the Atmospheres of Mars and Venus," *Icarus,* Vol. 21, No. 4, April 1974, pp. 496–505.

[9] Torrance, K. E., "Comparison of Finite-Difference Computations of Natural Convection," *Journal of Research of the National Bureau of Standards,* Vol. 72B, No. 4, Oct.–Dec. 1968, pp. 281–300.

[10] Spiegel, E. A. and Veronis, G., "On the Boussinesq Approximation for a Compressible Fluid," *Astrophysical Journal,* Vol. 131, No. 2, 1960, pp. 442–447.

[11] Cabelli, A. and Davis, G., "A Numerical Study of the Bénard Cell," *Journal of Fluid Mechanics,* Vol. 45, Pt 4, Feb. 1971, pp. 805–829.

[12] Emmons, H. W., "Critique of Numerical Modeling of Fluid-Mechanics Phenomena," *Annual Review of Fluid Mechanics,* Vol. 2, 1970, pp. 15–36 (Annual Reviews Inc., Palo Alto, Calif.).

[13] Moore, D. R. and Weiss, N. O., "Two-Dimensional Rayleigh-Bénard Convection," *Journal of Fluid Mechanics,* Vol. 58, Pt. 2, April 1973, pp. 289–312.

[14] Traugott, S. C., "An Improved Differential Approximation for Radiative Transfer with Spherical Symmetry," *AIAA Journal,* Vol. 7, No. 10, Oct. 1969, pp. 1825–1832.

[15] Traugott, S. C., "Radiation through a Plane-Parallel Absorbing Medium between Directional Surfaces," *AIAA Journal,* Vol. 9, No. 3, March 1971, pp. 500–507.

[16] Young, D., "Iterative Methods for Solving Partial Difference Equations of Elliptic Type," *Transactions of the American Mathematical Society,* Vol. 76, Jan. 1954, pp. 92–111.

[17] Torrance, K. E. and Rockett, J. A., "Numerical Study of Natural Convection," *Journal of Fluid Mechanics,* Vol. 36, Pt. 1, March 1969, pp. 33–54.

[18] Hauf, W. and Grigull, U., "Optical Methods in Heat Transfer," *Advances in Heat Transfer,* Vol. 6, Academic Press, New York, 1970, pp. 133–136.